Comput Mech (2016) 57:325–338
DOI 10.1007/s00466-015-1234-2

ORIGINAL PAPER

A variational formulation with rigid-body constraints for finite elasticity: theory, finite element implementation, and applications

Heng Chi[1] · **Oscar Lopez-Pamies**[2] · **Glaucio H. Paulino**[1]

Received: 26 May 2015 / Accepted: 26 November 2015 / Published online: 2 January 2016

Abstract This paper presents a new variational principle in finite elastostatics applicable to arbitrary elastic solids that may contain constitutively rigid spatial domains (e.g., rigid inclusions). The basic idea consists in describing the constitutive rigid behavior of a given spatial domain as a set of kinematic constraints over the boundary of the domain. From a computational perspective, the proposed formulation is shown to reduce to a set of algebraic constraints that can be implemented efficiently in terms of both single-field and mixed finite elements of arbitrary order. For demonstration purposes, applications of the proposed rigid-body-constraint formulation are illustrated within the context of elastomers, reinforced with periodic and random distributions of rigid filler particles, undergoing finite deformations.

Keywords Variational principles · Finite elastostatics · Constitutive constraints · Rigid inclusions

✉ Glaucio H. Paulino
paulino@gatech.edu

Heng Chi
hchi6@gatech.edu

Oscar Lopez-Pamies
pamies@illinois.edu

[1] School of Civil and Environmental Engineering, Georgia Institute of Technology, 790 Atlantic Drive, Atlanta, GA 30332, USA

[2] Department of Civil and Environmental Engineering, University of Illinois at Urbana-Champaign, 205 North Mathews Ave., Urbana, IL 61801, USA

1 Introduction

Synthetic elastomers are more often than not reinforced with filler particles (of various shapes) for engineering applications. The presence of stiff fillers is also ubiquitous in soft biological tissues. The nature of such fillers is motley, but they all typically exhibit a drastically stiffer mechanical response—about five orders of magnitude or possibly larger shear stiffness[1]—than then underlying soft matrix and consequently behave, for all practical purposes, as *rigid bodies*. The majority of existing computational studies of filler-reinforced soft materials in the literature (see, e.g., [8,13,15,18]) have opted for discretizing the stiff fillers with standard finite elements and assigning them a much stiffer constitutive response than that assigned to the surrounding matrix. For realistic types of material systems, the discretization of the underlying fillers takes up at least one fifth of the total number of degrees of freedom of the problem (see, e.g., [5]), thus increasing unnecessarily (since the fillers, again, do not experience any strain) the size of the system of the resulting discrete equations and, in turn, the computational cost. In an alternative approach, Chi et al. [5] have shown that, at least in two dimensions, stiff fillers can be discretized as single polygonal (n-gon) finite elements. Yet, fillers discretized as single polygonal elements, especially those with many (more than 100 edges) and/or with highly graded edges, are "mechanically softer" than standard elements and hence more prone to deform. Moreover, they require a numerical integration scheme of higher order than standard elements. While increasing the constitutive stiffness of single-polygonal-element fillers and enhancing the associ-

[1] For instance, the shear modulus of a typical rubber is in the order of 0.1 MPa while the shear modulus of carbon black is in the order of 10 GPa.

ated numerical integration scheme leads to accurate results, both of these remediations are computationally undesirable as they degrade the conditioning of the stiffness matrix and increase the computational cost.

The object of this paper is to put forth a new variational formulation in finite elastostatics whose finite-element implementation is free of the shortcomings of existing approaches, as outlined above, when dealing with elastic solids that contain rigid domains. The basic idea consists in describing the constitutive rigid behavior of a given spatial domain as a set of kinematic constraints over the boundary of the domain, thereby eluding their internal discretizaion. The idea is similar in nature to common multi-point constraint approaches, wherein the motion of a set of nodes is constrained by the motion of an assigned node or set of nodes. Contrary to these approaches, however, the formulation proposed here renders Lagrange multipliers of direct physical relevance which allow for the extraction of key information about the fields *within* the rigid domains, such as for instance their average stress.

The remainder of the paper is organized as follows. In Sect. 2, the standard displacement-based and mixed variational formulations of finite elastostatics are recalled. Section 3 presents the new variational formulation, while Sect. 4 presents its finite-element implementation. Section 5 illustrates applications of the proposed formulation to the numerical modeling of various types of filled elastomers. Finally, some concluding remarks are recorded in Sect. 6.

Before proceeding with the technical sections, we briefly and partially introduce the notation adopted in this paper. For any given variable (or field) g, be it a tensor of any order, we denote by δg its variation. For any function (or functional) $f(g)$ that depends on g, we write $\mathrm{D}f(g)\cdot\delta g$ to denote its derivative (or directional derivative) with respect to g. Moreover, for any subset E of a given spatial domain Ω, $E\subset\Omega$, we denote by $|E|$ its area or volume, by ∂E its boundary, and by $\langle\cdot\rangle_E$ the average operator:

$$\langle\cdot\rangle_E \doteq \frac{1}{|E|}\int_E (\cdot)\,\mathrm{d}\mathbf{X}. \tag{1}$$

If the average is taken over the whole domain Ω, we use instead the notation $\langle\cdot\rangle$ with the subscript Ω omitted. We shall also use $|\cdot|$ to denote the standard determinant operator of a matrix.

2 Preliminaries: classical variational formulations of finite elastostatics

Consider an elastic solid that, in its undeformed and stress-free configuration, occupies a domain Ω with boundary $\partial\Omega$. The part of the boundary $\partial\Omega^{\mathbf{X}}\subset\partial\Omega$ is assumed to be subjected to a prescribed displacement field $\mathbf{u}^0$, whereas the complementary part of the boundary $\partial\Omega^{\boldsymbol{\sigma}}$ is assumed to be subjected to a prescribed surface traction $\mathbf{t}$ (per unit undeformed surface). The presence of body forces is neglected. The constitutive response of the elastic solid is taken to be characterized by a hyperelastic energy W which is taken to be a non-negative, quasi-convex, and objective function of the deformation gradient tensor $\mathbf{F}$. Accordingly, the first Piola–Kirchhoff stress tensor $\mathbf{P}$ at each material point $\mathbf{X}\in\Omega$ is formally given by the constitutive relation

$$\mathbf{P}(\mathbf{X}) = \frac{\partial W}{\partial \mathbf{F}}(\mathbf{X},\mathbf{F}). \tag{2}$$

The displacement-based formulation The so-called displacement-based formulation of finite elastostatics considers the displacement field $\mathbf{u}$ as the only independent field; accordingly, the deformation gradient is written as $\mathbf{F}(\mathbf{u}) = \mathbf{I}+\nabla\mathbf{u}$, where ∇ denotes the gradient operator with respect to the undeformed configuration and $\mathbf{I}$ stands for the identity in the space of second-order tensors. The classical principle of minimum potential energy states that the equilibrium displacement field $\widehat{\mathbf{u}}$ is the field that minimizes the potential energy Π among the set of all kinematically admissible displacements $\mathbf{u}$, namely,

$$\Pi\left(\widehat{\mathbf{u}}\right) = \min_{\mathbf{u}\in\mathcal{K}(\Omega)}\Pi(\mathbf{u}) \tag{3}$$

with

$$\Pi(\mathbf{u}) = \int_\Omega W(\mathbf{X},\mathbf{F}(\mathbf{u}))\,\mathrm{d}\mathbf{X} - \int_{\partial\Omega^{\boldsymbol{\sigma}}}\mathbf{t}\cdot\mathbf{u}\mathrm{d}S, \tag{4}$$

where $\mathcal{K}(\Omega)$ stands for a sufficiently large set of kinematically admissible displacements $\mathbf{u}$ over Ω such that $\mathbf{u}=\mathbf{u}^0$ on $\partial\Omega^{\mathbf{X}}$.

The Euler–Lagrange equations associated with the variational problem (3)–(4) read, in weak form, as

$$\begin{aligned}\mathrm{D}\Pi\cdot\delta\mathbf{u} &= \int_\Omega \frac{\partial W}{\partial\mathbf{F}}(\mathbf{X},\mathbf{F}(\mathbf{u})) : \nabla(\delta\mathbf{u})\,\mathrm{d}\mathbf{X} - \int_{\partial\Omega^{\boldsymbol{\sigma}}}\mathbf{t}\cdot\delta\mathbf{u}\mathrm{d}S\\ &= 0 \quad \forall\delta\mathbf{u}\in\mathcal{K}^0(\Omega),\end{aligned} \tag{5}$$

where $\mathcal{K}^0(\Omega)$ is a subset of $\mathcal{K}(\Omega)$ that contains displacements that vanish on $\partial\Omega^{\mathbf{X}}$.

A mixed formulation Via the use of partial Legendre transforms, the above displacement-based formulation can be recast as a mixed variational formulation involving an additional hydrostatic pressure field p as unknown (see, e.g., [2–5,20,22]). More specifically, the most commonly

utilized mixed formulation[2] states that the pair of equilibrium displacement field $\hat{\mathbf{u}}$ and hydrostatic pressure field $\hat{p}$ is the solution to the following min–max problem among all kinematic admissible displacements $\mathbf{u}$ and hydrostatic pressures p:

$$\overline{\Pi}\left(\hat{\mathbf{u}}, \hat{p}\right) = \min_{\mathbf{u}\in\mathcal{K}(\Omega)} \max_{p\in\mathcal{Q}(\Omega)} \overline{\Pi}\left(\mathbf{u}, p\right) \tag{6}$$

with

$$\overline{\Pi}\left(\mathbf{u}, p\right) = \int_{\Omega} \left\{-\overline{W}^{*}\left(\mathbf{X}, \overline{\mathbf{F}}\left(\mathbf{u}\right), p\right) + p\left[\det \mathbf{F}\left(\mathbf{u}\right) - 1\right]\right\} \mathrm{d}\mathbf{X} - \int_{\partial\Omega^{\sigma}} \mathbf{t}\cdot\mathbf{u}\mathrm{d}S. \tag{7}$$

In these relations, $\mathcal{Q}\left(\Omega\right)$ stands for the set of all square integrable functions on Ω, $\overline{\mathbf{F}} = \left(\det \mathbf{F}\right)^{-\frac{1}{3}}\mathbf{F}$, and the associated complementary stored-energy function $\overline{W}^{*}\left(\mathbf{X}, \overline{\mathbf{F}}\left(\mathbf{u}\right), q\right)$ is defined by the partial Legendre transformation

$$\overline{W}^{*}\left(\mathbf{X}, \overline{\mathbf{F}}, p\right) = \max_{J}\left\{p\left(J-1\right) - \overline{W}\left(\mathbf{X}, \overline{\mathbf{F}}, J\right)\right\}, \tag{8}$$

where the function $\overline{W}\left(\mathbf{X}, \overline{\mathbf{F}}, J\right)$ is such that $W\left(\mathbf{X}, \mathbf{F}\right) = \overline{W}\left(\mathbf{X}, \overline{\mathbf{F}}, J\right)$ when $J = \det \mathbf{F}$.

The Euler–Lagrange equations associated with the variational principle (6)–(7) read, in weak form, as

$$\mathrm{D}\overline{\Pi}\cdot\delta\mathbf{u} = \int_{\Omega}\left[-\frac{\partial\overline{W}^{*}}{\partial\mathbf{F}}\left(\mathbf{X}, \overline{\mathbf{F}}\left(\mathbf{u}\right), p\right) + p\frac{\partial}{\partial\mathbf{F}}\left(\det\mathbf{F}(\mathbf{u})\right)\right] : \nabla\left(\delta\mathbf{u}\right)\mathrm{d}\mathbf{X} - \int_{\partial\Omega^{\sigma}}\mathbf{t}\cdot\delta\mathbf{u}\mathrm{d}S = 0 \quad \forall\delta\mathbf{u}\in\mathcal{K}^{0}\left(\Omega\right), \tag{9}$$

$$\mathrm{D}\overline{\Pi}\cdot\delta p = \int_{\Omega}\left[\det\mathbf{F}\left(\mathbf{u}\right) - 1 - \frac{\partial\overline{W}^{*}}{\partial p}\left(\mathbf{X}, \overline{\mathbf{F}}\left(\mathbf{u}\right), p\right)\right]\delta p\mathrm{d}\mathbf{X} = 0 \quad \forall\delta p\in\mathcal{Q}\left(\Omega\right). \tag{10}$$

3 The new variational formulation

Within the generic setting of the preceding section, we henceforth consider the case when the elastic solid contains a collection of N disconnected regions $\Omega_1^{(2)}, \ldots, \Omega_N^{(2)}$ that are constitutively rigid. Collectively, these regions occupy the domain $\Omega^{(2)} = \Omega_1^{(2)} \cup \cdots \cup \Omega_N^{(2)}$. The remaining non-rigid part of the solid is denoted by $\Omega^{(1)}$, so that $\Omega^{(1)} \cup \Omega^{(2)} = \Omega$ and $\Omega^{(1)} \cap \Omega^{(2)} = \varnothing$. The collection of interfaces of material discontinuity between the rigid and non-rigid domains is labeled as Γ. Further, the interface of material discontinuity between the rigid domain $\Omega_i^{(2)}$ and the non-rigid part of the solid $\Omega^{(1)}$ is denoted by Γ^i, so that $\Gamma^1 \cup \cdots \cup \Gamma^N = \Gamma$ and $\Gamma^1 \cap \cdots \cap \Gamma^N = \varnothing$; see Fig. 1 for a schematic of the solid of interest with the various geometric quantities indicated.

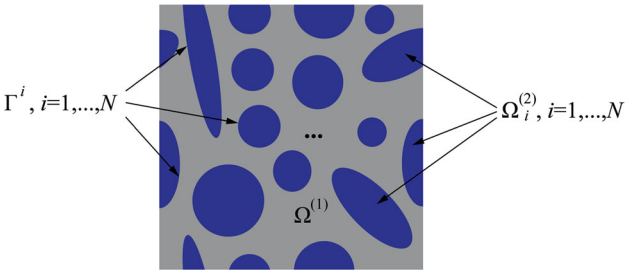

Fig. 1 Schematic of an elastic solid containing N disconnected regions $\Omega_1^{(2)}, \ldots, \Omega_N^{(2)}$ that are constitutively rigid. The interface of material discontinuity between the rigid domain $\Omega_i^{(2)}$ and the non-rigid part of the solid $\Omega^{(1)}$ is denoted by Γ^i

Having specified the geometric quantities of interest, the stored-energy function characterizing the constitutive response of the solid can be conveniently written in the form

$$W\left(\mathbf{X}, \mathbf{F}\right) = \left[1 - \chi\left(\mathbf{X}\right)\right]W^{(1)}\left(\mathbf{X}, \mathbf{F}\right) + \chi\left(\mathbf{X}\right)W^{(2)}\left(\mathbf{F}\right), \tag{11}$$

where the indicator function $\chi\left(\mathbf{X}\right)$ takes the value 1 if the position vector $\mathbf{X}\in\Omega^{(2)}$ and 0 otherwise, $W^{(1)}$ stands for the stored-energy function characterizing the constitutive (possibly heterogeneous) response of the non-rigid part of the solid, and

$$W^{(2)}\left(\mathbf{F}\right) = \begin{cases} 0 & \text{if} \quad \mathbf{F}\in Orth^{+} \\ +\infty & \text{otherwise} \end{cases} \tag{12}$$

with $Orth^{+}$ denoting the set of proper orthogonal second-order tensors.

Because of the kinematic constraint implied by the stored-energy function (12), the standard variational formulations (3)–(4) and (6)–(7) cannot be utilized directly. By exploiting the fact that the motion of the rigid domains can be fully described in terms solely of the motion of their boundaries, we propose to reformulate the problem so that the standard variational formulations are considered only in the non-rigid domain $\Omega^{(1)}$ with the constraint that the motion of each interface Γ^i be a rigid body motion.

The displacement-based formulation with rigid-body constraints Thus, within the context of a displacement-based formulation, the proposed variational statement involving constitutively rigid domains reads as

$$\Pi^{(1)}\left(\widehat{\mathbf{u}}\right) = \min_{\mathbf{u}\in\mathcal{K}^{R}\left(\Omega^{(1)}\right)} \Pi^{(1)}\left(\mathbf{u}\right) \tag{13}$$

[2] We note that different mixed variational principles which do not require any splitting of the deformation gradient into deviatoric ($\overline{\mathbf{F}}$) and volumetric ($\det\mathbf{F}$) parts are also available [5].

with

$$\Pi^{(1)}(\mathbf{u}) = \int_{\Omega^{(1)}} W^{(1)}(\mathbf{X}, \mathbf{F}(\mathbf{u}))\, \mathrm{d}\mathbf{X} - \int_{\partial\Omega^{\sigma}} \mathbf{t}\cdot\mathbf{u}\mathrm{d}S, \quad (14)$$

where the set $\mathcal{K}^R$ of kinematically admissible displacements is now given by

$$\begin{aligned}\mathcal{K}^R(\Omega^{(1)}) = \Big\{ & \mathbf{u} : \mathbf{u} \in \mathcal{K}\left(\Omega^{(1)}\right) \quad \text{and} \quad \mathbf{u} = \mathbf{u}_0^i + \mathbf{H}^i\mathbf{X}, \\ & \mathbf{H}^{iT}\mathbf{H}^i + \mathbf{H}^i + \mathbf{H}^{iT} = 0, \quad \mathbf{u}_0^i \in \mathbb{R}^d, \\ & \mathbf{H}^i \in \mathbb{R}^{d\times d} \text{ on } \Gamma^i, \quad i = 1,\ldots,N\Big\}. \end{aligned} \quad (15)$$

We note that the constant vector $\mathbf{u}_0^i$ and constant second-order tensor $\mathbf{H}^i$ in (15) characterize the rigid body translation and rotation of the rigid domain $\Omega_i^{(2)}$. Further, once the equilibrium displacement field $\widehat{\mathbf{u}}$ has been computed from (13)–(15) for all material points $\mathbf{X} \in \Omega^{(1)}$, the equilibrium displacement field at any material point *within* each rigid domain $\Omega_i^{(2)}$ can be readily determined from the affine relation $\widehat{\mathbf{u}} = \widehat{\mathbf{u}}_0^i + \widehat{\mathbf{H}}^i\mathbf{X}$.

By introducing two sets of Lagrange multipliers, $\boldsymbol{\lambda}^i$ and $\boldsymbol{\Sigma}^i$, $i = 1,\ldots,N$, taken here to be, respectively, continuous vector fields and constant symmetric second-order tensors, the above constrained minimization problem can be recast as the following constraint-free stationary principle:

$$\min_{\mathbf{u}\in\mathcal{K}(\Omega^{(1)})} \min_{\mathbf{u}_0^i\in\mathbb{R}^d} \min_{\mathbf{H}^i\in\mathbb{R}^{d\times d}} \operatorname{stat}_{\boldsymbol{\lambda}^i\in[C^0(\Gamma^i)]^d} \operatorname{stat}_{\boldsymbol{\Sigma}^i\in\mathbb{R}^{d\times d}_{symm}} \mathcal{L}\left(\mathbf{u}, \mathbf{u}_0^i, \mathbf{H}^i, \boldsymbol{\lambda}^i, \boldsymbol{\Sigma}^i\right) \quad (16)$$

with

$$\begin{aligned}\mathcal{L}\left(\mathbf{u}, \mathbf{u}_0^i, \mathbf{H}^i, \boldsymbol{\lambda}^i, \boldsymbol{\Sigma}^i\right) = \Pi^{(1)}(\mathbf{u}) + \sum_{i=1}^{N} \frac{1}{2}|\Omega_i^{(2)}|\boldsymbol{\Sigma}^i : \\ \left(\mathbf{H}^{iT}\mathbf{H}^i + \mathbf{H}^i + \mathbf{H}^{iT}\right) + \sum_{i=1}^{N}\int_{\Gamma^i} \boldsymbol{\lambda}^i \cdot \left(\mathbf{u} - \mathbf{u}_0^i - \mathbf{H}^i\mathbf{X}\right)\mathrm{d}S. \end{aligned} \quad (17)$$

The strong form of the Euler–Lagrange equations associated with this last variational principle are given by

$$\operatorname{Div}\mathbf{P}(\mathbf{X}) = \mathbf{0} \quad \text{in } \Omega^{(1)}, \quad (18)$$

$$\mathbf{P}(\mathbf{X})\,\mathbf{N} = \mathbf{t} \quad \text{on } \partial\Omega^{\sigma}, \quad (19)$$

$$\boldsymbol{\lambda}^i - \mathbf{P}(\mathbf{X})\,\mathbf{N}^{\Gamma} = \mathbf{0} \quad \text{on } \Gamma^i, \quad i = 1,\ldots,N, \quad (20)$$

$$\int_{\Gamma_i} \boldsymbol{\lambda}^i \mathrm{d}S = \mathbf{0} \qquad i = 1,\ldots,N, \quad (21)$$

$$\left(\mathbf{H}^i + \mathbf{I}\right)\boldsymbol{\Sigma}^i = \frac{1}{|\Omega_i^{(2)}|}\int_{\Gamma^i}\left(\boldsymbol{\lambda}^i \otimes \mathbf{X}\right)\mathrm{d}S \quad i = 1,\ldots,N, \quad (22)$$

$$\mathbf{u} = \mathbf{u}_0^i + \mathbf{H}^i\mathbf{X} \quad \text{on } \Gamma^i, \quad i = 1,\ldots,N, \quad (23)$$

$$\mathbf{H}^{iT}\mathbf{H}^i + \mathbf{H}^i + \mathbf{H}^{iT} = \mathbf{0} \quad i = 1,\ldots,N, \quad (24)$$

where it is recalled that $\mathbf{P}(\mathbf{X}) = \partial W(\mathbf{X}, \mathbf{F}(\mathbf{u}))/\partial\mathbf{F}$ is the first Piola–Kirchhoff stress tensor, $\mathbf{N}$ is the outward unit normal vector on $\partial\Omega^{\sigma}$, and $\mathbf{N}^{\Gamma}$ is the unit normal vector on Γ pointing towards the non-rigid domain. From (20) and (21), we deduce that the Lagrange multiplier field $\boldsymbol{\lambda}^i$ corresponds to the traction on the interface Γ^i. Moreover, it follows from (22) and the divergence theorem that the Lagrange multiplier field $\boldsymbol{\Sigma}^i$ is directly associated with the volume average of the first Piola–Kirchhoff stress over the rigid domain $\Omega_i^{(2)}$ via the relation

$$\left(\mathbf{H}^i + \mathbf{I}\right)\boldsymbol{\Sigma}^i = \langle\mathbf{P}(\mathbf{X})\rangle_{\Omega_i^{(2)}} \quad i = 1,\ldots,N. \quad (25)$$

It is worthwhile noting that the above-proposed formulation shares similarities with the variational treatment of boundary conditions in computational homogenization problems (see, e.g., [10,16,17]). Indeed, the ability of the proposed method to provide information about the stress field within the rigid domains is important for such problems, and of the essence in analyses of damage such as filler/matrix debonding.

For later use in their finite-element implementation, it proves convenient to record here the above Euler–Lagrange equations in weak form:

$$\begin{aligned}\mathrm{D}\mathcal{L}\cdot\delta\mathbf{u} = & \int_{\Omega^{(1)}} \frac{\partial W^{(1)}}{\partial\mathbf{F}}(\mathbf{X}, \mathbf{F}(\mathbf{u})) : \nabla(\delta\mathbf{u})\,\mathrm{d}\mathbf{X} \\ & - \int_{\partial\Omega^{\sigma}} \mathbf{t}\cdot\delta\mathbf{u}\mathrm{d}S + \sum_{i=1}^{N}\int_{\Gamma^i} \boldsymbol{\lambda}^i\cdot\delta\mathbf{u}\mathrm{d}S = 0 \quad \forall\delta\mathbf{u}\in\mathcal{K}^0\left(\Omega^{(1)}\right), \end{aligned} \quad (26)$$

$$\mathrm{D}\mathcal{L}\cdot\delta\mathbf{u}_0^i = \int_{\Gamma^i}\boldsymbol{\lambda}^i\cdot\delta\mathbf{u}_0^i\mathrm{d}S = 0 \quad \forall\delta\mathbf{u}_0^i \in \mathbb{R}^d, \quad (27)$$

$$\begin{aligned}\mathrm{D}\mathcal{L}\cdot\delta\mathbf{H}^i = & |\Omega_i^{(2)}|\left(\mathbf{H}^i + \mathbf{I}\right)\boldsymbol{\Sigma}^i : \delta\mathbf{H}^i - \int_{\Gamma^i}\left(\boldsymbol{\lambda}^i\otimes\mathbf{X}\right) : \\ & \delta\mathbf{H}^i\mathrm{d}S = 0 \quad \forall\delta\mathbf{H}^i \in \mathbb{R}^{d\times d}, \end{aligned} \quad (28)$$

$$\begin{aligned}\mathrm{D}\mathcal{L}\cdot\delta\boldsymbol{\lambda}^i = & \int_{\Gamma^i}\left(\mathbf{u} - \mathbf{u}_0^i - \mathbf{H}^i\mathbf{X}\right)\cdot\delta\boldsymbol{\lambda}^i\mathrm{d}S = 0 \quad \forall\delta\boldsymbol{\lambda}^i \\ & \in \left[C^0\left(\Gamma^i\right)\right]^d, \end{aligned} \quad (29)$$

$$\begin{aligned}\mathrm{D}\mathcal{L}\cdot\delta\boldsymbol{\Sigma}^i = & \frac{1}{2}|\Omega_i^{(2)}|\left(\mathbf{H}^{iT}\mathbf{H}^i + \mathbf{H}^i + \mathbf{H}^{iT}\right) : \delta\boldsymbol{\Sigma}^i = 0 \\ & \forall\delta\boldsymbol{\Sigma}^i \in \mathbb{R}^{d\times d}_{\mathrm{symm}}. \end{aligned} \quad (30)$$

A mixed formulation with rigid-body constraints Similarly, within the context of the standard mixed variational formulation recalled in Sect. 2, the proposed variational statement involving constitutively rigid domains reads as

$$\overline{\Pi}^{(1)}\left(\widehat{\mathbf{u}},\widehat{p}\right)=\min_{\mathbf{u}\in\mathcal{K}^R\left(\Omega^{(1)}\right)}\max_{p\in\mathcal{Q}\left(\Omega^{(1)}\right)}\overline{\Pi}^{(1)}\left(\mathbf{u},p\right) \tag{31}$$

with

$$\overline{\Pi}^{(1)}\left(\mathbf{u},p\right)=\int_{\Omega^{(1)}}\left\{-\overline{W}^{(1)*}\left(\mathbf{X},\overline{\mathbf{F}}\left(\mathbf{u}\right),p\right)+p\left[\det\mathbf{F}\left(\mathbf{u}\right)-1\right]\right\}\mathrm{d}\mathbf{X}-\int_{\partial\Omega^{\sigma}}\mathbf{t}\cdot\mathbf{u}\mathrm{d}S, \tag{32}$$

where it is recalled that $\overline{\mathbf{F}}=\left(\det\mathbf{F}\right)^{-\frac{1}{3}}\mathbf{F}$, $\overline{W}^{(1)*}\left(\overline{\mathbf{F}}\left(\mathbf{u}\right),p\right)$ is the partial Legendre transformation (8) associated with the stored-energy function $W^{(1)}$ of the non-rigid domain $\Omega^{(1)}$, and, again, $\mathcal{K}^R$ stands for the set of constrained displacements (15) while $\mathcal{Q}$ stands for the set of all square integrable functions on $\Omega^{(1)}$.

Following the use of Lagrange multipliers $\boldsymbol{\lambda}^i$ and $\boldsymbol{\Sigma}^i$ much like in the preceding displacement-based approach, the constrained min–max problem (31)–(32) can be recast as an equivalent stationary principle free of constraints:

$$\min_{\mathbf{u}\in\mathcal{K}\left(\Omega^{(1)}\right)}\ \min_{\mathbf{u}_0^i\in\mathbb{R}^d}\ \min_{\mathbf{H}^i\in\mathbb{R}^{d\times d}}\ \operatorname*{stat}_{\boldsymbol{\lambda}^i\in[C^0(\Gamma^i)]^d}\ \operatorname*{stat}_{\boldsymbol{\Sigma}^i\in\mathbb{R}^{d\times d}_{symm}}\ \max_{p\in\mathcal{Q}\left(\Omega^{(1)}\right)}\overline{\mathcal{L}}\left(\mathbf{u},\mathbf{u}_0^i,\mathbf{H}^i,\boldsymbol{\lambda}^i,\boldsymbol{\Sigma}^i,p\right) \tag{33}$$

with

$$\overline{\mathcal{L}}\left(\mathbf{u},\mathbf{u}_0^i,\mathbf{H}^i,\boldsymbol{\lambda}^i,\boldsymbol{\Sigma}^i,p\right)=\overline{\Pi}^{(1)}\left(\mathbf{u},p\right)+\sum_{i=1}^{N}\frac{1}{2}|\Omega_i^{(2)}|\boldsymbol{\Sigma}^i:\left(\mathbf{H}^{iT}\mathbf{H}^i+\mathbf{H}^i+\mathbf{H}^{iT}\right)+\sum_{i=1}^{N}\int_{\Gamma^i}\boldsymbol{\lambda}^i\cdot\left(\mathbf{u}-\mathbf{u}_0^i-\mathbf{H}^i\mathbf{X}\right)\mathrm{d}S. \tag{34}$$

The weak form of the Euler–Lagrange equations (for conciseness, we do not spell out their strong form) of this variational problem read as

$$\mathrm{D}\overline{\mathcal{L}}\cdot\delta\mathbf{u}=\int_{\Omega^{(1)}}\left[-\frac{\partial\overline{W}^{(1)*}}{\partial\mathbf{F}}\left(\mathbf{X},\overline{\mathbf{F}}\left(\mathbf{u}\right),p\right)+p\frac{\partial}{\partial\mathbf{F}}\left(\det\mathbf{F}(\mathbf{u})\right)\right]:\nabla\left(\delta\mathbf{u}\right)\mathrm{d}\mathbf{X}-\int_{\partial\Omega^{\sigma}}\mathbf{t}\cdot\delta\mathbf{u}\mathrm{d}S+\sum_{i=1}^{N}\int_{\Gamma^i}\boldsymbol{\lambda}^i\cdot\delta\mathbf{u}\mathrm{d}S=0$$
$$\forall\delta\mathbf{u}\in\mathcal{K}^0\left(\Omega^{(1)}\right), \tag{35}$$

$$\mathrm{D}\overline{\mathcal{L}}\cdot\delta\mathbf{u}_0^i=\int_{\Gamma^i}\boldsymbol{\lambda}^i\cdot\delta\mathbf{u}_0^i\mathrm{d}S=0\quad\forall\delta\mathbf{u}_0^i\in\mathbb{R}^d, \tag{36}$$

$$\mathrm{D}\overline{\mathcal{L}}\cdot\delta\mathbf{H}^i=|\Omega_i^{(2)}|\left(\mathbf{H}^i+\mathbf{I}\right)\boldsymbol{\Sigma}^i:\delta\mathbf{H}^i-\int_{\Gamma^i}\left(\boldsymbol{\lambda}^i\otimes\mathbf{X}\right):\delta\mathbf{H}^i\mathrm{d}S=0\quad\forall\delta\mathbf{H}^i\in\mathbb{R}^{d\times d}, \tag{37}$$

$$\mathrm{D}\overline{\mathcal{L}}\cdot\delta\boldsymbol{\lambda}^i=\int_{\Gamma^i}\left(\mathbf{u}-\mathbf{u}_0^i-\mathbf{H}^i\mathbf{X}\right)\cdot\delta\boldsymbol{\lambda}^i\mathrm{d}S=0\quad\forall\delta\boldsymbol{\lambda}^i\in\left[C^0\left(\Gamma^i\right)\right]^d, \tag{38}$$

$$\mathrm{D}\overline{\mathcal{L}}\cdot\delta\boldsymbol{\Sigma}^i=\frac{1}{2}|\Omega_i^{(2)}|\left(\mathbf{H}^{iT}\mathbf{H}^i+\mathbf{H}^i+\mathbf{H}^{iT}\right):\delta\boldsymbol{\Sigma}^i=0\quad\forall\delta\boldsymbol{\Sigma}^i\in\mathbb{R}^{d\times d}_{\mathrm{symm}}, \tag{39}$$

$$\mathrm{D}\overline{\mathcal{L}}\cdot\delta p=\int_{\Omega^{(1)}}\left[\det\mathbf{F}\left(\mathbf{u}\right)-1-\frac{\partial\overline{W}^{(1)*}}{\partial p}\left(\mathbf{X},\overline{\mathbf{F}}\left(\mathbf{u}\right),p\right)\right]\delta p\mathrm{d}\mathbf{X}=0\quad\forall\delta p\in\mathcal{Q}\left(\Omega^{(1)}\right). \tag{40}$$

Here too the Lagrange multiplier field $\boldsymbol{\lambda}^i$ corresponds to the traction field on the interface Γ^i, whereas $\boldsymbol{\Sigma}^i$ is related to the volume average of the first Piola–Kirchhoff stress over $\Omega_i^{(2)}$ via relation (25).

4 Finite element implementation

In this section, we outline the finite element approximation and implementation of the proposed variational formulation (see, e.g., [1,9,24,25]). Given that the numerical examples that will be discussed in Sect. 5 are for conditions of plane strain, we restrict the presentation to two dimensions (2D) and simply note that the extension to three dimensions (3D) is straightforward, a brief discussion of which can be found in the Appendix.

We begin by considering a partition Ω_h of the domain Ω occupied by the elastic solid in which the discretization of the non-rigid domain, $\Omega_h^{(1)}$, consists of non-overlapping polygonal elements of arbitrary number of vertices $n\geq 3$ (the standard triangular and quadrilateral elements are thus included as special cases). Each rigid discrete domain $\Omega_{i\,h}^{(2)}$ consists of a polygon that is characterized by the discretization of its boundary Γ_h^i. The area encompassed by Γ_h^i shall be denoted by A^i. An example of such a discretization is shown in Fig. 2.

The corresponding discrete displacement space $\mathcal{K}_{h,k}$ in the non-rigid domain is defined as

$$\mathcal{K}_{h,k}=\left\{\mathbf{u}_h\in[C^0\left(\Omega_h^{(1)}\right)]^2\cap\mathcal{K}\left(\Omega^{(1)}\right):\mathbf{u}_h|_E\in[\mathcal{V}_k\left(E\right)]^2,\ \forall E\in\Omega_h^{(1)}\right\}, \tag{41}$$

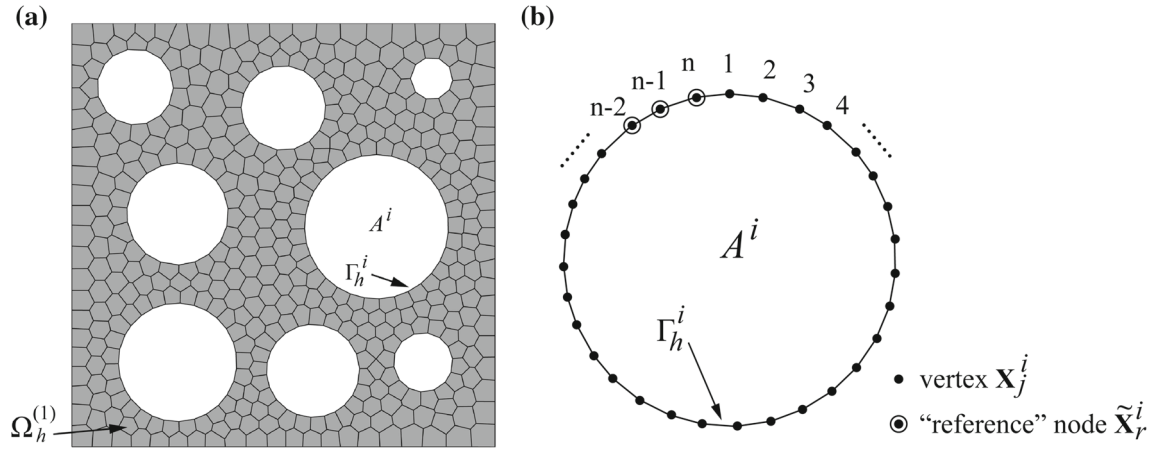

Fig. 2 An example of the discretization considered in this paper. **a** The discretized non-rigid domain $\Omega_h^{(1)}$ is a regular polygonal mesh and each rigid domain corresponds to a polygon that is characterized by the discretization of its boundary Γ_h^i. **b** An illustration of the ith rigid domain, of area A^i, with n vertices

where $\mathcal{V}_k(E)$ is the finite element space defined over element E, which satisfies

$$\mathcal{P}_k(E) \subseteq \mathcal{V}_k(E), \tag{42}$$

and whose functions possess $k$the order variation on ∂E. $\mathcal{P}_k(E)$ is the kth order polynomial space. We also define the discrete space of piecewise continuous polynomial functions up to order k on Γ_h^i, denoted as $\mathcal{W}_k\left(\Gamma_h^i\right)$. For use in the mixed formulation, we further define a discrete pressure space,

$$\mathcal{Q}_{h,k-1} = \left\{ p_h \in \mathcal{Q}\left(\Omega_h^{(1)}\right) : p_h|_E \in \mathcal{P}_{k-1}(E), \forall E \in \Omega_h^{(1)} \right\}. \tag{43}$$

Finite element approximation of the displacement-based formulation Having defined the discrete spaces, the conforming Galerkin approximation of Eqs. (26)–(30) amounts to finding $\widehat{\mathbf{u}}_h \in \mathcal{K}_{h,k}$, $\widehat{\boldsymbol{\lambda}}_h^i \in \left[\mathcal{W}_k\left(\Gamma_h^i\right)\right]^2$, $\widehat{\mathbf{u}}_0^i \in \mathbb{R}^2$, $\widehat{\boldsymbol{\Sigma}}^i \in \mathbb{R}^{2\times 2}_{\text{symm}}$, and $\widehat{\mathbf{H}}^i \in \mathbb{R}^{2\times 2}$ that solve the following system of nonlinear algebraic equations:

$$\mathrm{D}\mathcal{L}_h \cdot \delta\mathbf{u}_h = \fint_{\Omega_h^{(1)}} \frac{\partial W^{(1)}}{\partial \mathbf{F}}\left(\mathbf{X}, \mathbf{F}(\mathbf{u}_h)\right) : \nabla(\delta\mathbf{u}_h)\,\mathrm{d}\mathbf{X} - \oint_{\partial\Omega^\sigma} \mathbf{t}\cdot\delta\mathbf{u}_h \mathrm{d}S + \sum_{i=1}^{N} \oint_{\Gamma_h^i} \boldsymbol{\lambda}_h^i \cdot \delta\mathbf{u}_h \mathrm{d}S = 0 \quad \forall \delta\mathbf{u}_h \in \mathcal{K}_{h,k}^0, \tag{44}$$

$$\mathrm{D}\mathcal{L}_h \cdot \delta\mathbf{u}_0^i = \oint_{\Gamma_h^i} \boldsymbol{\lambda}_h^i \cdot \delta\mathbf{u}_0^i \mathrm{d}S = 0 \quad \forall \delta\mathbf{u}_0^i \in \mathbb{R}^2, \tag{45}$$

$$\mathrm{D}\mathcal{L}_h \cdot \delta\mathbf{H}^i = A_i\left(\mathbf{H}^i + \mathbf{I}\right)\boldsymbol{\Sigma}^i : \delta\mathbf{H}^i - \oint_{\Gamma_h^i}\left(\boldsymbol{\lambda}_h^i \otimes \mathbf{X}\right) : \delta\mathbf{H}^i \mathrm{d}S = 0 \quad \forall \delta\mathbf{H}^i \in \mathbb{R}^{2\times 2}, \tag{46}$$

$$\mathrm{D}\mathcal{L}_h \cdot \delta\boldsymbol{\lambda}_h^i = \oint_{\Gamma_h^i}\left(\mathbf{u}_h - \mathbf{u}_0^i - \mathbf{H}^i\mathbf{X}\right)\cdot\delta\boldsymbol{\lambda}_h^i \mathrm{d}S = 0 \quad \forall \delta\boldsymbol{\lambda}_h^i \in \left[\mathcal{W}_k\left(\Gamma_h^i\right)\right]^2, \tag{47}$$

$$\mathrm{D}\mathcal{L}_h \cdot \delta\boldsymbol{\Sigma}^i = \frac{1}{2}A_i\left(\mathbf{H}^{iT}\mathbf{H}^i + \mathbf{H}^i + \mathbf{H}^{iT}\right) : \delta\boldsymbol{\Sigma}^i = 0 \quad \forall \delta\boldsymbol{\Sigma}^i \in \mathbb{R}^{2\times 2}_{\text{symm}}. \tag{48}$$

In the above equations, we have made use of the notation $\fint_{\Omega_h^{(1)}} = \sum_{E\in\Omega_h^{(1)}} \fint_E$ to indicate standard numerical evaluation of the integrals over $\Omega_h^{(1)}$, which account for elemental contributions following the standard assembly rules (see, e.g., [1,9,24,25]), and the symbol $\oint$ to indicate the numerical evaluation of integrals over external ($\partial\Omega_h$) and internal boundaries (Γ_h^i).

The system of Eqs. (44)–(48) can be rewritten in a more computationally efficient manner, as described next. By applying the nodal integration rule, we begin by noting that the boundary integrals

$$\oint_{\Gamma_h^i} \delta\boldsymbol{\lambda}_h^i \cdot \left(\mathbf{u}_h - \mathbf{u}_0^i - \mathbf{H}^i\mathbf{X}\right)\mathrm{d}S, \tag{49}$$

$$\oint_{\Gamma_h^i} \boldsymbol{\lambda}_h^i \cdot \left(\delta\mathbf{u}_h - \delta\mathbf{u}_0^i - \delta\mathbf{H}^i\mathbf{X}\right)\mathrm{d}S \tag{50}$$

take the form

$$\oint_{\Gamma_h^i} \delta\boldsymbol{\lambda}_h^i \cdot \left(\mathbf{u}_h - \mathbf{u}_0^i - \mathbf{H}^i\mathbf{X}\right)\mathrm{d}S = \sum_{\mathbf{X}_j^i \in \Gamma_h^i}\left[w_j^i \delta\boldsymbol{\lambda}_{h,j}^i \cdot \left(\mathbf{u}_{h,j}^i - \mathbf{u}_0^i - \mathbf{H}^i\mathbf{X}_j^i\right)\right], \tag{51}$$

$$\oint_{\Gamma_h^i} \boldsymbol{\lambda}_h^i \cdot \left(\delta \mathbf{u}_h - \delta \mathbf{u}_0^i - \delta \mathbf{H}^i \mathbf{X}\right) \mathrm{d}S = \sum_{\mathbf{X}_j^i \in \Gamma_h^i} \left[w_j^i \boldsymbol{\lambda}_{h,j}^i \cdot \left(\delta \mathbf{u}_{h,j}^i - \delta \mathbf{u}_0^i - \delta \mathbf{H}^i \mathbf{X}_j^i\right)\right], \tag{52}$$

where w_j^i is the weight associated with vertex $\mathbf{X}_j^i$ of the chosen nodal quadrature rule. In addition to the nodal displacement $\mathbf{u}_{h,j}^i = \left\{u_{hx,j}^i, u_{hy,j}^i\right\}^T$ and Lagrange multiplier $\boldsymbol{\lambda}_{h,j}^i = \left\{\lambda_{hx,j}^i, \lambda_{hy,j}^i\right\}^T$, these approximations involve the unknown variables $\mathbf{u}_0^i$ and $\mathbf{H}^i$. It turns out that it is possible to condense these variables from (44)–(48) by introducing a set of "reference" nodes on Γ_h^i. In the present 2D context, only three non-collinear "reference" nodes are needed per interface Γ_h^i; see Fig. 2b. Indeed, let us assume that we have three non-collinear "reference" nodes for the interface Γ_h^i, denoted as $\widetilde{\mathbf{X}}_r^i = \left\{\tilde{x}_r^i, \tilde{y}_r^i\right\}^T, r = 1, 2, 3$. It follows that any linear field $g(\mathbf{X})$ can be interpolated exactly via

$$g(\mathbf{X}) = \sum_{r=1}^{3} \phi_k^i(\mathbf{X})\, \widetilde{g}_{,r}^i, \tag{53}$$

where the notation $\widetilde{g}_{,j}^i = g\left(\widetilde{\mathbf{X}}_j^i\right)$ has been introduced for convenience and

$$\phi_1^i(\mathbf{X}) = \frac{\begin{vmatrix} 1 & x & y \\ 1 & \tilde{x}_2^i & \tilde{y}_2^i \\ 1 & \tilde{x}_3^i & \tilde{y}_3^i \end{vmatrix}}{\widetilde{\phi}^i}, \qquad \phi_2^i(\mathbf{X}) = \frac{\begin{vmatrix} 1 & \tilde{x}_1^i & \tilde{y}_1^i \\ 1 & x & y \\ 1 & \tilde{x}_3^i & \tilde{y}_3^i \end{vmatrix}}{\widetilde{\phi}^i},$$
$$\phi_3^i(\mathbf{X}) = \frac{\begin{vmatrix} 1 & \tilde{x}_1^i & \tilde{y}_1^i \\ 1 & \tilde{x}_2^i & \tilde{y}_2^i \\ 1 & x & y \end{vmatrix}}{\widetilde{\phi}^i} \tag{54}$$

with

$$\widetilde{\phi}^i = \begin{vmatrix} 1 & \tilde{x}_1^i & \tilde{y}_1^i \\ 1 & \tilde{x}_2^i & \tilde{y}_2^i \\ 1 & \tilde{x}_3^i & \tilde{y}_3^i \end{vmatrix}, \tag{55}$$

and $\mathbf{X} = \{x, y\}^T$. With help of the function representation (53), the unknown fields $\mathbf{u}_0^i$ and $\mathbf{H}^i$ can be written as

$$\mathbf{u}_0^i + \mathbf{H}^i \mathbf{X} = \sum_{r=1}^{3} \phi_r^i(\mathbf{X})\, \widetilde{\mathbf{u}}_{,r}^i. \tag{56}$$

Upon recognizing that

$$\delta\widetilde{\boldsymbol{\lambda}}_{h,r}^i \cdot \left[\widetilde{\mathbf{u}}_{h,r}^i - \mathbf{u}_0^i - \mathbf{H}^i \widetilde{\mathbf{X}}_r^i\right] = 0,$$
$$\widetilde{\boldsymbol{\lambda}}_{h,r}^i \cdot \left[\delta\widetilde{\mathbf{u}}_{h,r}^i - \delta\mathbf{u}_0^i - \delta\mathbf{H}^i \widetilde{\mathbf{X}}_r^i\right] = 0, \tag{57}$$

the right hand sides of relations (51) and (52) can then be rewritten in the form

$$\sum_{\mathbf{X}_j^i \in \Gamma_h^i / \left\{\widetilde{\mathbf{X}}_1^i, \widetilde{\mathbf{X}}_2^i, \widetilde{\mathbf{X}}_3^i\right\}} \left[w_j^i \delta\boldsymbol{\lambda}_{h,j}^i \cdot \left(\mathbf{u}_{h,j}^i - \sum_{r=1}^{3} \phi_{r,j}^i \mathbf{u}_{h,r}^i\right)\right], \tag{58}$$

$$\sum_{\mathbf{X}_j^i \in \Gamma_h^i / \left\{\widetilde{\mathbf{X}}_1^i, \widetilde{\mathbf{X}}_2^i, \widetilde{\mathbf{X}}_3^i\right\}} \left[w_j^i \boldsymbol{\lambda}_{h,j}^i \cdot \left(\delta\mathbf{u}_{h,j}^i - \sum_{r=1}^{3} \phi_{r,j}^i \delta\mathbf{u}_{h,r}^i\right)\right]. \tag{59}$$

Now, by defining arrays $\delta\boldsymbol{\Lambda}^i \in \mathbb{R}^{2n-6}$, $\mathbf{U}^i \in \mathbb{R}^{2n}$ such that

$$\delta\boldsymbol{\Lambda}^i = \left\{ w_1^i \delta\lambda_{hx,1}^i \quad w_1^i \delta\lambda_{hy,1}^i \quad \cdots \quad w_{n-3}^i \delta\lambda_{hx,n-3}^i \quad w_{n-3}^i \delta\lambda_{hy,n-3}^i \right\}^T, \tag{60}$$

$$\mathbf{U}^i = \left\{ u_{hx,1}^i \quad u_{hy,1}^i \quad \cdots \quad u_{hx,n-3}^i \quad u_{hy,n-3}^i \;\middle|\; \widetilde{u}_{hx,1}^i \quad \widetilde{u}_{hy,1} \quad \cdots \right\}^T, \tag{61}$$

and the $2n-6 \times 2n$ matrix $\mathbf{C}^i$ with entries

$$\mathbf{C}^i = \left[\begin{array}{ccc|ccccc} 1 & \cdots & 0 & -\phi_{1,1}^i & 0 & \cdots & -\phi_{3,1}^i & 0 \\ & & & 0 & -\phi_{1,1}^i & \cdots & 0 & -\phi_{3,1}^i \\ \vdots & \ddots & \vdots & & & & \vdots & \\ & & & -\phi_{1,n-3}^i & 0 & \cdots & -\phi_{3,n-3}^i & 0 \\ 0 & \cdots & 1 & 0 & -\phi_{1,n-3}^i & \cdots & 0 & -\phi_{3,n-3}^i \end{array}\right], \tag{62}$$

we have that

$$\sum_{\mathbf{X}_j^i \in \Gamma_h^i / \left\{\widetilde{\mathbf{X}}_1^i, \widetilde{\mathbf{X}}_2^i, \widetilde{\mathbf{X}}_3^i\right\}} \left[w_j^i \delta\boldsymbol{\lambda}_{h,j}^i \cdot \left(\mathbf{u}_{h,j}^i - \sum_{r=1}^{3} \phi_{r,j}^i \mathbf{u}_{h,r}^i\right)\right] = \delta\boldsymbol{\Lambda}^{iT} \mathbf{C}^i \mathbf{U}^i. \tag{63}$$

Similarly, the matrix representation

$$\sum_{\mathbf{X}_j^i \in \Gamma_h^i / \left\{\widetilde{\mathbf{X}}_1^i, \widetilde{\mathbf{X}}_2^i, \widetilde{\mathbf{X}}_3^i\right\}} \left[w_j^i \boldsymbol{\lambda}_{h,j}^i \cdot \left(\delta\mathbf{u}_{h,j}^i - \sum_{r=1}^{3} \phi_{r,j}^i \delta\mathbf{u}_{h,r}^i\right)\right] = \delta\mathbf{U}^{iT} \mathbf{C}^{iT} \boldsymbol{\Lambda}^i \tag{64}$$

follows from the definitions

$$\boldsymbol{\Lambda}^i = \left\{ w_1^i \lambda_{hx,1}^i \quad w_1^i \lambda_{hy,1}^i \quad \cdots \quad w_{n-3}^i \lambda_{hx,n-3}^i \quad w_{n-3}^i \lambda_{hy,n-3}^i \right\}^T \tag{65}$$

and

$$\delta\mathbf{U}^i = \left\{\delta u^i_{hx,1} \quad \delta u^i_{hy,1} \quad \cdots \quad \delta u^i_{hx,n-3} \;\middle|\; \delta v^i_{hy,n-3} \quad \delta\widetilde{u}^i_{hx,1} \quad \delta\widetilde{u}_{hy,1} \quad \cdots\right\}^T. \tag{66}$$

For reference, we further introduce the matrix gradient relations

$$\mathbf{H}^i = \begin{bmatrix} \widetilde{u}^i_{x,1} & \widetilde{u}^i_{x,2} & \widetilde{u}^i_{x,3} \\ \widetilde{u}^i_{y,1} & \widetilde{u}^i_{y,2} & \widetilde{u}^i_{y,3} \end{bmatrix} \begin{bmatrix} \partial\phi^i_1/\partial x & \partial\phi^i_1/\partial y \\ \partial\phi^i_2/\partial x & \partial\phi^i_2/\partial y \\ \partial\phi^i_3/\partial x & \partial\phi^i_3/\partial y \end{bmatrix} = \widetilde{\mathbf{U}}^i\mathbf{B}^i \tag{67}$$

and

$$\delta\mathbf{H}^i = \begin{bmatrix} \delta\widetilde{u}^i_{x,1} & \delta\widetilde{u}^i_{x,2} & \delta\widetilde{u}^i_{x,3} \\ \delta\widetilde{u}^i_{y,1} & \delta\widetilde{u}^i_{y,2} & \delta\widetilde{u}^i_{y,3} \end{bmatrix} \begin{bmatrix} \partial\phi^i_1/\partial x & \partial\phi^i_1/\partial y \\ \partial\phi^i_2/\partial x & \partial\phi^i_2/\partial y \\ \partial\phi^i_3/\partial x & \partial\phi^i_3/\partial y \end{bmatrix} = \delta\widetilde{\mathbf{U}}^i\mathbf{B}^i. \tag{68}$$

In view of the above development, the Galerkin finite element Eqs. (44)–(48) can be finally recast in the more compact form

$$\begin{aligned} \mathrm{D}\mathcal{L}_h\cdot\delta\mathbf{u}_h = {} & \int\!\!\!\!\!\!\square_{\Omega_h^{(1)}} \frac{\partial W^{(1)}}{\partial\mathbf{F}}\left(\mathbf{X},\mathbf{F}\left(\mathbf{u}_h\right)\right) : \nabla\left(\delta\mathbf{u}_h\right)\mathrm{d}\mathbf{X} \\ & - \oint_{\partial\Omega_h^{\sigma}} \mathbf{t}\cdot\delta\mathbf{u}_h\mathrm{d}S \\ & + \sum_{i=1}^{N} A^i\left(\widetilde{\mathbf{U}}^i\mathbf{B}^i\right)\boldsymbol{\Sigma}^i : \left(\delta\widetilde{\mathbf{U}}^i\mathbf{B}^i\right) \\ & + \sum_{i=1}^{N} \delta\mathbf{U}^{iT}\mathbf{C}^{iT}\boldsymbol{\Lambda}^i = 0, \quad \forall\delta\mathbf{u}_h \in \mathcal{K}^0_{h,k}, \end{aligned} \tag{69}$$

$$\mathrm{D}\mathcal{L}_h\cdot\delta\boldsymbol{\Sigma}^i = \frac{1}{2}A^i\left(\mathbf{B}^{iT}\widetilde{\mathbf{U}}^{iT}\widetilde{\mathbf{U}}^i\mathbf{B}^i + \widetilde{\mathbf{U}}^i\mathbf{B}^i + \mathbf{B}^{iT}\widetilde{\mathbf{U}}^{iT}\right) : \delta\boldsymbol{\Sigma}^i = 0, \quad \forall\delta\boldsymbol{\Sigma}^i \in \mathbb{R}^{2\times2}_{\mathrm{symm}}, \tag{70}$$

$$\mathrm{D}\mathcal{L}_h\cdot\delta\boldsymbol{\Lambda}^i = \delta\boldsymbol{\Lambda}^{iT}\mathbf{C}^i\mathbf{U}^i = 0, \quad \forall\delta\boldsymbol{\Lambda}^i \in \mathbb{R}^{2n-6}. \tag{71}$$

Finite element approximation of the mixed formulation The conforming Galerkin approximation of Eqs. (26)–(28) for the mixed formulation can be constructed by essentially following the same procedure described above for the displacement-based formulation. For conciseness, we only present the final result here. The problem reduces to finding the pair of unknowns $\left(\hat{\mathbf{u}}_h, \hat{p}_h\right) \in \mathcal{K}_{h,k} \times \mathcal{Q}_{h,k-1}$, symmetric tensors $\widehat{\boldsymbol{\Sigma}}^i \in \mathbb{R}^{2\times2}_{\mathrm{symm}}$, and Lagrange multiplier arrays $\widehat{\boldsymbol{\Lambda}}^i \in \mathbb{R}^2$ that solve the following system of nonlinear algebraic equations:

$$\begin{aligned} \mathrm{D}\overline{\mathcal{L}}_h\cdot\delta\mathbf{u}_h = {} & \int\!\!\!\!\!\!\square_{\Omega_h^{(1)}} \left[\frac{-\partial\overline{W}^{*(1)}}{\partial\mathbf{F}}\left(\mathbf{X},\mathbf{F}\left(\mathbf{u}_h\right),p_h\right) \right. \\ & \left. + p_h\frac{\partial}{\partial\mathbf{F}}\left(\det\mathbf{F}\left(\mathbf{u}_h\right)\right)\right] : \nabla\left(\delta\mathbf{u}_h\right)\mathrm{d}\mathbf{X} \\ & - \oint_{\partial\Omega_h^{\sigma}} \mathbf{t}\cdot\delta\mathbf{u}_h\mathrm{d}S + \sum_{i=1}^{N} A^i\left(\widetilde{\mathbf{U}}^i\mathbf{B}^i\right)\boldsymbol{\Sigma}^i : \left(\delta\widetilde{\mathbf{U}}^i\mathbf{B}^i\right) \\ & + \sum_{i=1}^{N} \delta\mathbf{U}^{iT}\mathbf{C}^{iT}\boldsymbol{\Lambda}^i = 0, \quad \forall\delta\mathbf{u}_h \in \mathcal{K}^0_{h,k}\left(\Omega^{(1)}\right), \end{aligned} \tag{72}$$

$$\mathrm{D}\overline{\mathcal{L}}_h\cdot\delta p_h = \int\!\!\!\!\!\!\square_{\Omega_h^{(1)}} \left[\det\mathbf{F}\left(\mathbf{u}_h\right) - 1 - \frac{\partial\overline{W}^{*(1)}}{\partial p}\left(\mathbf{X},\overline{\mathbf{F}}\left(\mathbf{u}_h\right),p_h\right)\right]\delta p_h = 0, \quad \forall\delta p_h \in \mathcal{Q}_{h,k-1}\left(\Omega^{(1)}\right), \tag{73}$$

$$\mathrm{D}\overline{\mathcal{L}}_h\cdot\delta\boldsymbol{\Sigma}^i = \frac{1}{2}A^i\left(\mathbf{B}^{iT}\widetilde{\mathbf{U}}^{iT}\widetilde{\mathbf{U}}^i\mathbf{B}^i + \widetilde{\mathbf{U}}^i\mathbf{B}^i + \mathbf{B}^{iT}\widetilde{\mathbf{U}}^{iT}\right) : \delta\boldsymbol{\Sigma}^i = 0, \quad \forall\delta\boldsymbol{\Sigma}^i \in \mathbb{R}^{2\times2}_{\mathrm{symm}}, \tag{74}$$

$$\mathrm{D}\overline{\mathcal{L}}_h\cdot\delta\boldsymbol{\lambda}^i = \delta\boldsymbol{\Lambda}^{iT}\mathbf{C}^i\mathbf{U}^i, \quad \forall\delta\boldsymbol{\Lambda}^i \in \mathbb{R}^{2n-6}. \tag{75}$$

Three points are worth remarking regarding the discrete displacement-based (69)–(71) and mixed (72)–(75) formulations:

- Neither formulation requires numerical integration of the terms associated with the rigid domains. In fact, for both displacement-based and mixed approximations, the characterization of the motion of each rigid region is formulated as a set of algebraic equations constraining the displacement degrees of freedom (DOFs) on their interface Γ^i_h. For a given interface Γ^i_h with n boundary nodes, there are $2n-3$ constraining equations, $2n-6$ of which [Eqs. (71), (75)] are linear on the displacement DOFs—and thus can be handled with great efficiency using methods such as transformation and elimination of dependent variables (see. e.g, [6,14,23])—and 3 of which [Eqs. (70), (74)] are quadratic on the displacement DOFs of the chosen "reference" nodes; we emphasize that although Eqs. (70) and (74) describe 4 constraints, only 3 of them are independent because of the symmetry of $\boldsymbol{\Sigma}^i$.
- The Lagrange multiplier $\boldsymbol{\Lambda}^i$ associated with Eqs. (71) and (75) is not an array of nodal tractions, but an array instead of the products of nodal tractions and the weights of their corresponding nodes. Therefore, we do not need to specify explicitly the nodal weights in (51) and (52), since they are implicitly incorporated in $\boldsymbol{\Lambda}^i$.

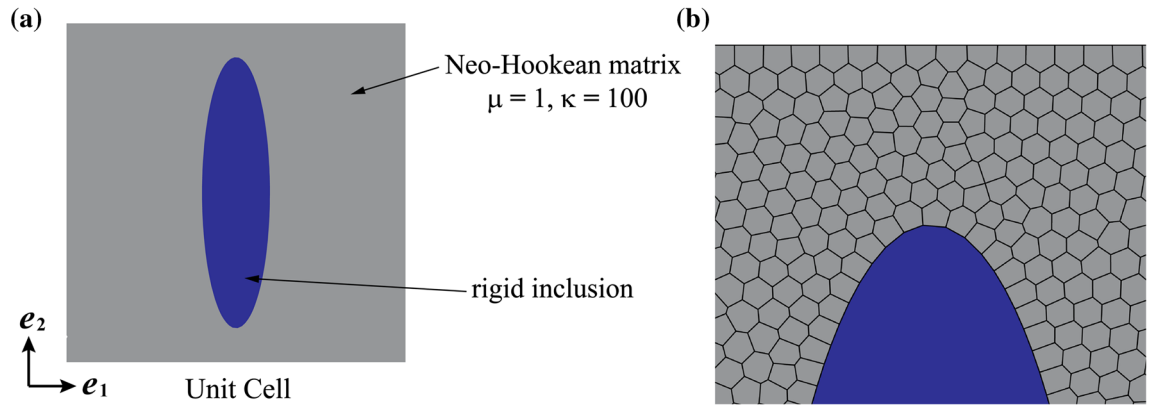

Fig. 3 **a** The unit cell considered in this example. **b** The corresponding polygonal discretization consisting of 3000 linear displacement-based polygonal elements and 6132 nodes

- By construction, the formulations (69)–(71) and (72)–(75) are expected to be more robust and efficient than existing approaches that make use of the internal discretization of rigid domains. The numerical examples presented in the following section suggest that this is indeed the case.

5 Numerical examples

In the sequel, we deploy the above-developed formulation to study: (i) the nonlinear elastic response of a compressible elastomer reinforced with a periodic distribution of rigid elliptical particles under simple shear, and (ii) the nonlinear elastic response of an incompressible elastomer reinforced with a random isotropic distribution of rigid circular particles under uniaxial tension. These numerical examples are aimed at showcasing the capabilities of the proposed formulation to deal with rigid domains of arbitrary shapes and arbitrary spatial distributions, as well as to confirm its higher robustness and efficiency when compared with existing approaches.

Throughout this section, polygonal discretizations and polygonal finite element approximations are adopted, since they have been shown to be inherently suited to describe large deformations [5]. A triangulation integration scheme is employed, which subdivides each polygonal element into triangles and applies the Dunavant rules [7] in each of the subdivided triangles (see, e.g., [5,21]). Unless otherwise stated, the order of the triangulation scheme is chosen to be 2, implying that the scheme can integrate any polynomial functions over the element exactly up to 2nd order. In addition, the standard Newton-Raphson algorithm is used to solve the relevant nonlinear systems of equations. In each loading step, the convergence criterion is set such that the norm of the residual reduces below 10^{-8} times that of the initial residual.

5.1 Elastomers reinforced with a periodic distribution of rigid elliptical particles

Our first example is concerned with the nonlinear elastic response of a compressible elastomer reinforced with a periodic distribution of rigid elliptical particles under simple shear, where the macroscopic deformation gradient has the form $\langle \mathbf{F} \rangle = \mathbf{I} + \gamma \mathbf{e}_1 \otimes \mathbf{e}_2$ with γ denoting the applied macroscopic shear. Since the microstructure is periodic, it suffices (at least up to the onset of instabilities [15]) to consider the response of a simple unit cell under periodic boundary conditions. The unit cell considered in our calculations is depicted in Fig. 3a. We restrict attention to the case of elliptical particles of aspect ratio 4, area fraction $c = 15\,\%$, that are initially aligned with the laboratory frame of reference $\mathbf{e}_1$–$\mathbf{e}_2$. The elastomeric matrix is taken as a compressible Neo-Hookean material with stored-energy function

$$W(\mathbf{F}) = \left[\overline{\mathbf{F}} : \overline{\mathbf{F}} - 3\right] + \frac{\kappa}{2} (\det \mathbf{F} - 1)^2 , \tag{76}$$

where μ and κ stand, respectively, for the initial shear and bulk moduli of the elastomer. For definiteness, we take $\mu = 1$ and $\kappa = 100$. In this case, periodic boundary conditions imply that

$$\begin{aligned} u_k(1, X_2) - u_k(0, X_2) &= \langle \mathbf{F} \rangle_{k1} - \delta_{k1} \\ u_k(X_1, 1) - u_k(X_1, 0) &= \langle \mathbf{F} \rangle_{k2} - \delta_{k2} \quad \forall k = 1, 2, \end{aligned} \tag{77}$$

where δ_{kl} is the Kronecker delta, whereas u_k and $X_k (k = 1, 2)$ are the components of the displacement field and initial position vector in a Cartesian frame of reference with its origin placed at the left lower corner of the unit cell (see, e.g., [13]).

In terms of the discretization, we consider the polygonal mesh depicted in Fig. 3b. It consists of 3000 polygonal elements and 6132 nodes. To be able to apply the periodic boundary conditions (77), we adopt the concept introduced

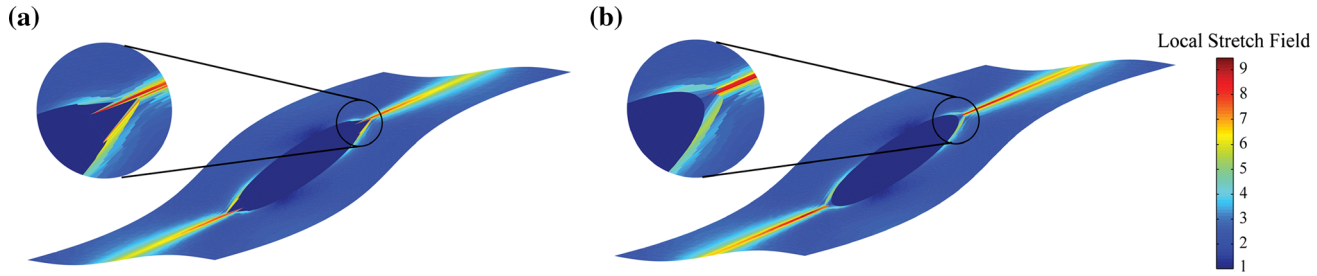

Fig. 4 **a** An illustration of the insufficiency of the 2nd triangulation scheme in the "n-gon" approach, which treats the elliptical particle as a stiff but deformable polygonal element, at an applied shear of $\gamma = 2$. The element deforms at the *top* and *bottom* poles of the particle, where the local stretches in the particle-matrix interface are highest. **b** With a 6th order triangulation scheme, the particle element remains rigid at the same level of applied shear

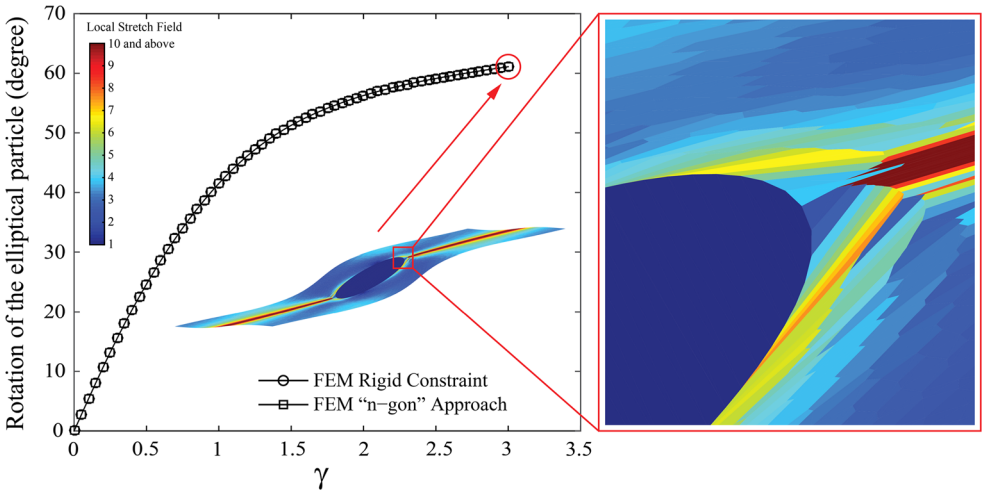

Fig. 5 The finite deformation of the rigid elliptical particle as a function of applied shear γ. The *inset* depicts the deformed shape of the unit cell at $\gamma = 3$ using the rigid-body constraint approach

in [5] of locally inserting additional nodes to achieve periodic nodal distributions on opposite boundaries. A first order displacement-based finite element formulation is utilized.

In addition to results from the proposed displacement-based formulation with rigid-body constraints, for comparison purposes, we also work out results based on the "n-gon" approach introduced in [5]. In the "n-gon" approach, the rigid behavior of the particle is approximated by considering it as a compressible Neo-Hookean solid with $\mu = \kappa = 10^6$. We find that moduli higher than 10^6 would lead to larger converged residual norms that would make the convergence criterion harder to be satisfied. In terms of the size of the problem, the rigid-body constraint formulation leads to a system containing 12,893 DOFs, as compared to the one having 12,632 DOFs in the "n-gon" approach. We note that, although the size of the system obtained from the rigid-body constraint formulation is slightly larger than the one from the "n-gon" approach, most of the additional DOFs (258 DOFs) are Lagrange multipliers associated with linear constraints that can, as already indicated, be condensed from the system. Furthermore, the "n-gon" approach in this example treats the elliptical particle as a polygonal element with 132 edges. As mentioned in the Introduction, it is numerically challenging to make a polygonal element with many edges behave rigidly under large deformations, even with shear and bulk moduli as high as $\mu = \kappa = 10^6$. The adopted 2nd order triangulation scheme is insufficient for the particle element in this example and undesirable deformation occurs in highly stretched regions, such as the ones at the top and bottom of the elliptical particle, as shown in Fig. 4a. To overcome such difficulties, integration schemes of higher order are needed. We find that at least a 6th order triangulation scheme is needed to keep the particle rigid during the whole deformation process, as shown in Fig. 4b. This, however, increases the computational cost, given that the 6th order triangulation scheme requires many more integration points (1584 integration points) than the 2nd order one (396 integration points). By contrast, again, the rigid-body constraint approach treats the presence of the rigid particles, regardless of the number of edges, as a set of algebraic equations. Therefore, no numerical integration

Table 1 Summary of analysis histories and computational expenses of example 1

Approaches	# of Int. points	Aver. iter. per step	Time (S)
Rigid-body constraint	53,415	4.15	1007
"n-gon" approach	54,999	5.88	1350

is needed. Figure 5 shows the deformed configuration at $\gamma = 3$ of the unit cell obtained with the rigid-body constraint approach. As shown by the figure, the elliptical particle simply rotates under the applied shear while remaining rigid. Moreover, as a quantitative comparison, we also plot the rotating angle of the elliptical particle as a function of the applied amount of shear in Fig. 5 for the results obtained by the "n-gon" approach (with the 6th order triangulation rule in the particle) and rigid-body constraint approach.

We conclude this example by comparing the computational costs, shown in Table 1, associated with the "n-gon" approach and with the proposed approach with rigid-body constraints. We find that the proposed approach takes less computational time to reach the final deformation state (e.g., $\gamma = 3$) than the "n-gon" approach. Further, as a consequence of the algebraic nature of the constraining equations, the rigid-body constraint formulation uses less integration points than the "n-gon" approach. We also find that the rigid-body constraint formulation yields better conditioned finite element systems because it is free of the artificial high moduli (e.g., $\mu = \kappa = 10^6$) assigned to the particle. In turn, it takes less iterations per loading step to solve the nonlinear system of equations than the "n-gon" approach. These observed favorable comparisons, in view of the preceding discussion, indicate that the proposed rigid-body constraint formulation is indeed more robust and efficient than the "n-gon" approach.

5.2 Elastomers reinforced with a random distribution of circular particles

In this second example, we deploy the proposed mixed formulation to study the nonlinear elastic response of an incompressible elastomer filled with an isotropic distribution of rigid circular particles under uniaxial tension. The macroscopic deformation gradient has thus the form $\langle \mathbf{F} \rangle = \lambda \mathbf{e}_1 \otimes \mathbf{e}_1 + \lambda^{-1} \mathbf{e}_2 \otimes \mathbf{e}_2$ with λ denoting the macroscopic stretch in the tensile direction. To this end, we consider the filled elastomer to be comprised of the periodic repetition of a unit cell that contains a random distribution of a large number of particles constructed by means of a random sequential adsorption algorithm [13,19]. Motivated by the polydispersity in size of typical fillers (see, e.g., [11]), we consider in particular a case when there are three families of particles with radii

$$\left\{r^{(1)}, r^{(2)}, r^3\right\} = \{r, 0.75r, 0.5r\}$$

$$\text{with} \quad r = \left(\frac{c^{(1)}}{N^{(1)}\pi}\right)^{(1/2)}, \quad \text{and} \tag{78}$$

$$\left\{c^{(1)}, c^{(2)}, c^{(3)}\right\} = \{0.5c, 0.3c, 0, 2c\}, \tag{79}$$

where $N^{(1)}$ is the number of particles with the largest radius $r^{(1)}$, and c stands for the total are fraction of particles. In the present example, we take $N^{(1)} = 20$ and $c = 0.35$. A realization of such a unit cell containing a total number of 75 particles at area fraction $c = 35\,\%$ is shown in Fig. 6a. The elastomeric matrix is taken to be an incompressible Neo-Hookean material with stored-energy function

$$W(\mathbf{F}) = \begin{cases} \dfrac{\mu}{2}[\mathbf{F} : \mathbf{F} - 3] & \text{if} \quad \det \mathbf{F} = 1 \\ +\infty & \text{otherwise} \end{cases} \tag{80}$$

with shear modulus $\mu = 1$.

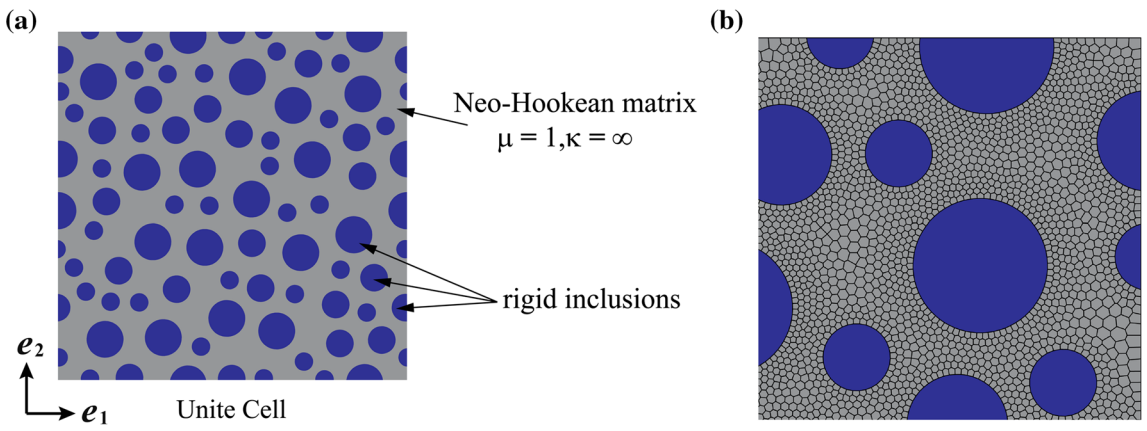

Fig. 6 **a** A realization of the type of unit cells considered in this example. **b** The corresponding polygonal discretization consisting of 20,000 linear mixed polygonal elements and 40,196 nodes

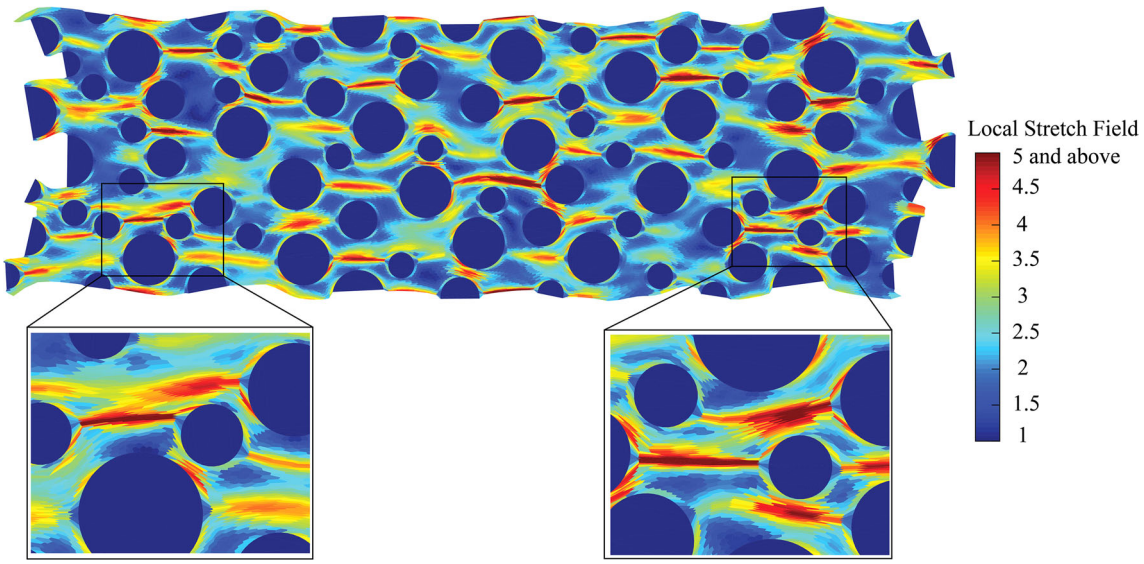

Fig. 7 Deformed configuration of the unit cell at the macroscopic stretch $\lambda = 1.8$

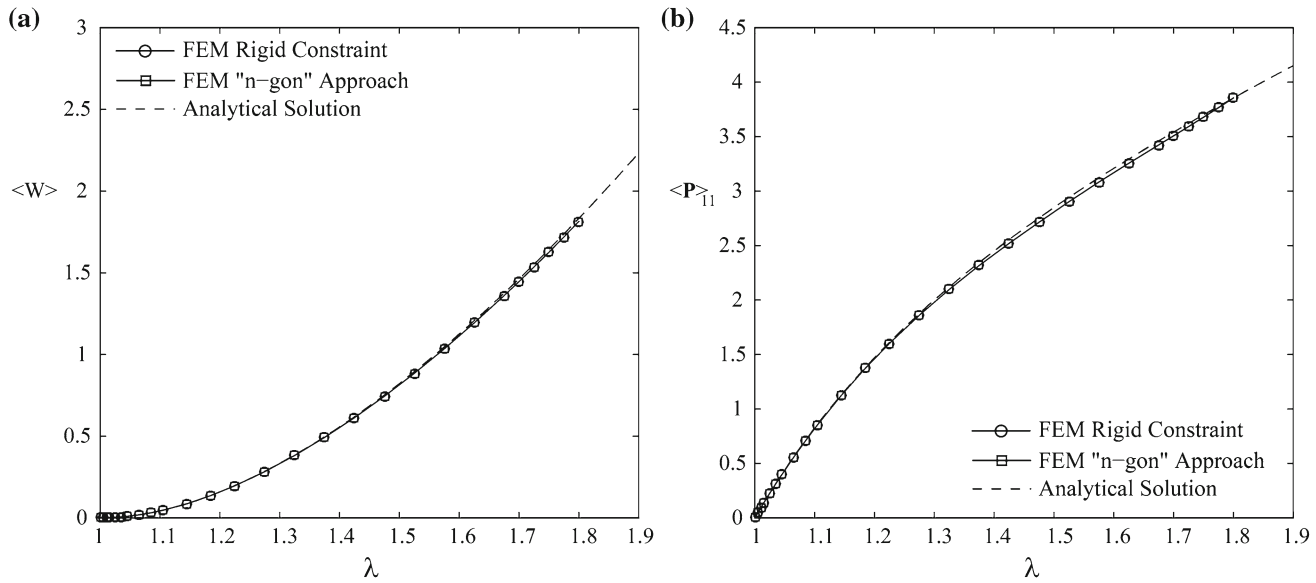

Fig. 8 Macroscopic response of the elastomer filled with a random isotropic distribution of rigid circular particles. **a** The total elastic energy density $\langle W \rangle$ versus the applied stretch λ. **b** The macroscopic stress $\langle \mathbf{P} \rangle_{11}$ versus the applied stretch λ

In terms of the discretization, we make use of linear mixed polygonal elements, which feature piecewise constant pressure field per element [5]. Figure 6b depicts a representative mesh containing a total of 20,000 elements and 40,196 nodes. As in the foregoing example, the mesh is also modified locally to achieve periodic nodal distributions on opposite boundaries by inserting additional nodes. The discretization results in a system of 107,635 DOFs with the rigid-body constraint formulation as compared to one of 100,481 DOFs with the "n-gon" approach. Again, most of the additional DOFs (6976 DOFs) in the rigid-body constraint formulation are Lagrange multipliers associated with linear constraints.

Much like in the preceding example, in addition to results from the proposed mixed formulation with rigid-body constraints, for comparison purposes, we also work out results based on the "n-gon" approach. In the latter approach, the rigid behavior of the particles are approximated by considering them as incompressible Neo-Hookean solids with shear modulus $\mu = 10^5$.

Figure 7 depicts the deformed configuration of the unit cell at an applied stretch of $\lambda = 1.8$ obtained by the rigid-body constraint approach, including the maximum stretch of each element. An immediate observation from the fringe plot is that, although most regions surrounding the particles

Table 2 Summary of analysis histories and computational expenses of example 2

Approaches	# of Int. points	Aver. iter. per step	Time (S)
Rigid-body constraint	349,137	4.08	3250
"n-gon" approach	360,402	4.96	4032

are highly stretched, all the particles remain unstrained, indicating the effectiveness of the proposed formulation to deal with complex spatial distributions of rigid domains. Figure 8a, b plot, respectively, the total elastic energy density $\langle W \rangle$ and the component of the macroscopic first Piola-Kirchoff stress $\langle \mathbf{P} \rangle_{11}$, as functions of the applied stretch λ for both approaches. In the rigid-body constraint approach, the macroscopic stress $\langle \mathbf{P} \rangle_{11}$ is computed from the finite element solution for the stress in the matrix phase in conjunction with the set of Lagrange multipliers $\mathbf{\Sigma}^i$ and relation (25). Both approaches produce identical macroscopic responses and they are in good agreement with the existing analytical solution of such a problem in the literature [12].

Similarly to the preceding example, the computational cost analysis summarized in Table 2 corroborates the higher robustness and efficiency of the proposed rigid-body constraint formulation, as it requires less integration points, takes less iterations per loading step, and uses less computational time than the "n-gon" approach.

6 Concluding remarks

In this work, we have introduced a simple yet general variational principle in finite elastostatics that, contrary to existing principles, is applicable to elastic solids that may contain constitutively rigid spatial domains. The presence of rigid domains is formulated as a combination of linear and nonlinear kinematic constraints on their boundary, whose associated Lagrange multipliers are directly related to the surface traction field and the volume average of the first Piola–Kirchhoff stress within each of the rigid domains. From a computational point of view, as compared to the commonly used approaches of discretizing the rigid domains with standard (triangular/tetrahedral or quadrilateral/hexahedral) finite elements, the proposed formulation does not require any discretization in the interior of each rigid domain. Furthermore, unlike the recently proposed "n-gon" approach, which needs special care in choosing the order of numerical integration and assigning material properties to accurately approximate rigid behavior, the proposed formulation is shown to reduce to a set of algebraic equations of the boundary displacement DOFs of each rigid domain, which can be implemented efficiently with either displacement-based or mixed finite elements of arbitrary orders, and lead to better conditioned nonlinear finite element systems. Although the size of the system obtained from the proposed rigid-body constraint formulation is slightly larger than the one from the "n-gon" approach, the majority of the additional DOFs are Lagrange multipliers associated with linear constraints that can be condensed from the system. Two numerical examples have been discussed to showcase the application of the proposed rigid-body constraint formulation and to demonstrate the effectiveness and efficiency of the approach in modeling elastomers filled with rigid particles of arbitrary shapes and spatial distributions. As a final remark, we point out that although the rigid-body formulation has been studied here in the context of elastostatics, it can be readily extended to elastodynamics, inelastic materials, and other physics problems.

Acknowledgments We acknowledge the support from the US National Science Foundation (NSF) through Grant CMMI #1559595 (formerly #1437535). The information presented in this paper is the sole opinion of the authors and does not necessarily reflect the views of the sponsoring agency.

Appendix: On the FE implementation in 3D

This appendix briefly describes the generalization of the FE implementation of the proposed rigid-body-constraint formulation to 3D. In this case, a set of four non-coplanar "reference" nodes is needed for each interface Γ_h^i (in 3D, Γ_h^i is the boundary of a polyhedral $\Omega_{ih}^{(2)}$). Assuming that we have four non-coplanar "reference" nodes for the interface Γ_h^i, denoted as $\widetilde{\mathbf{X}}_r^i = \left\{\tilde{x}_r^i, \tilde{y}_r^i, \tilde{z}_r^i\right\}^T$, $r = 1, 2, 3, 4$, any linear field $g(\mathbf{X})$ can be interpolated exactly via

$$g(\mathbf{X}) = \sum_{r=1}^{4} \phi_r^i(\mathbf{X})\, \widetilde{g}_{,r}^i, \tag{81}$$

where the interpolation functions are of the form

$$\phi_1^i(\mathbf{X}) = \frac{\begin{vmatrix} 1 & x & y & z \\ 1 & \tilde{x}_2^i & \tilde{y}_2^i & \tilde{z}_2^i \\ 1 & \tilde{x}_3^i & \tilde{y}_3^i & \tilde{z}_3^i \\ 1 & \tilde{x}_4^i & \tilde{y}_4^i & \tilde{z}_4^i \end{vmatrix}}{\widetilde{\phi}^i}, \quad \phi_2^i(\mathbf{X}) = \frac{\begin{vmatrix} 1 & \tilde{x}_1^i & \tilde{y}_1^i & \tilde{z}_1^i \\ 1 & x & y & z \\ 1 & \tilde{x}_3^i & \tilde{y}_3^i & \tilde{z}_3^i \\ 1 & \tilde{x}_4^i & \tilde{y}_4^i & \tilde{z}_4^i \end{vmatrix}}{\widetilde{\phi}^i}, \tag{82}$$

$$\phi_3^i(\mathbf{X}) = \frac{\begin{vmatrix} 1 & \tilde{x}_1^i & \tilde{y}_1^i & \tilde{z}_1^i \\ 1 & \tilde{x}_2^i & \tilde{y}_2^i & \tilde{z}_2^i \\ 1 & x & y & z \\ 1 & \tilde{x}_4^i & \tilde{y}_4^i & \tilde{z}_4^i \end{vmatrix}}{\widetilde{\phi}^i}, \quad \phi_4^i(\mathbf{X}) = \frac{\begin{vmatrix} 1 & \tilde{x}_1^i & \tilde{y}_1^i & \tilde{z}_1^i \\ 1 & \tilde{x}_2^i & \tilde{y}_2^i & \tilde{z}_2^i \\ 1 & \tilde{x}_3^i & \tilde{y}_3^i & \tilde{z}_3^i \\ 1 & x & y & z \end{vmatrix}}{\widetilde{\phi}^i} \tag{83}$$

with

$$\widetilde{\phi}^i = \begin{vmatrix} 1 & \widetilde{x}_1^i & \widetilde{y}_1^i & \widetilde{z}_1^i \\ 1 & \widetilde{x}_2^i & \widetilde{y}_2^i & \widetilde{z}_2^i \\ 1 & \widetilde{x}_3^i & \widetilde{y}_3^i & \widetilde{z}_3^i \\ 1 & \widetilde{x}_4^i & \widetilde{y}_4^i & \widetilde{z}_4^i \end{vmatrix}, \tag{84}$$

and $\mathbf{X} = \{x, y, z\}^T$. With help of (81), the unknown fields $\mathbf{u}_0^i$ and $\mathbf{H}^i$ can be written as

$$\mathbf{u}_0^i + \mathbf{H}^i \mathbf{X} = \sum_{r=1}^{4} \phi_k^i(\mathbf{X})\, \widetilde{\mathbf{u}}_{,r}^i \tag{85}$$

with $\widetilde{\mathbf{u}}_{,r}^i = \left\{ \widetilde{u}_{x,r}^i, \widetilde{u}_{y,r}^i, \widetilde{u}_{z,r}^i \right\}^T$. The remainder of the generalizations for both displacement-based and mixed approximations can be obtained by simply expanding the dimensions of nodal variables (and consequently, the corresponding arrays and matrices), and following the same procedure described for the 2D case. For conciseness, they are not presented here. As a final remark, we note that there is a total of $3n-6$ constraining equations for a given interface Γ_h^i with n boundary nodes in 3D. Moreover, $3n-12$ of the constraining equations are linear on the displacement DOFs (corresponding to Eqs. (71), (75) in 2D), and the remaining 6 are quadratic on the displacement DOFs of the "reference" nodes (corresponding to Eqs. (70), (74) in 2D).

References

1. Bonet J, Wood RD (2008) Nonlinear continuum mechanics for finite element analysis. Cambridge University Press, Cambridge
2. Brink U, Stein E (1996) On some mixed finite element methods for incompressible and nearly incompressible finite elasticity. Comput Mech 19(1):105–119
3. Chang TYP, Saleeb AF, Li G (1991) Large strain analysis of rubber-like materials based on a perturbed lagrangian variational principle. Comput Mech 8(4):221–233
4. Chen JS, Han W, Wu CT, Duan W (1997) On the perturbed Lagrangian formulation for nearly incompressible and incompressible hyperelasticity. Comput Methods Appl Mech Eng 142(3):335–351
5. Chi H, Talischi C, Lopez-Pamies O, Paulino GH (2015) Polygonal finite elements for finite elasticity. Int J Numer Methods Eng 101:305–328
6. Cook RD, Malkus DS, Plesha ME, Witt RJ (2002) Concepts and applications of finite element analysis, 4th edn. Wiley, New York
7. Dunavant D (1985) High degree efficient symmetrical gaussian quadrature rules for the triangle. Int J Numer Methods Eng 21(6):1129–1148
8. Goudarzi T, Spring DW, Paulino GH, Lopez-Pamies O (2015) Filled elastomers: a theory of filler reinforcement based on hydrodynamic and interphasial effects. J Mech Phys Solids. 80:37–67
9. Hughes TJR (2012) The finite element method: linear static and dynamic finite element analysis. Courier Dover Publications, Mineola
10. Kouznetsova V, Geers M, Brekelmans W (2004) Multi-scale secondorder computational homogenization of multi-phase materials: a nested finite element solution strategy. Comput Methods Appl Mech Eng 193(48):5525–5550
11. Leblanc JL (2010) Filled polymers: science and industrial applications. CRC Press, Boca Raton
12. Lopez-Pamies O (2010) An exact result for the macroscopic response of particle-reinforced Neo-Hookean solids. J Appl Mech 77(2):021016
13. Lopez-Pamies O, Goudarzi T, Danas K (2013) The nonlinear elastic response of suspensions of rigid inclusions in rubber: II—a simple explicit approximation for finite-concentration suspensions. J Mech Phys Solids 61:19–37
14. Luenberger DG (1973) Introduction to linear and nonlinear programming, vol 28. Addison-Wesley, Reading
15. Michel J-C, Lopez-Pamies O, Ponte Castañeda P, Triantafyllidis N (2010) Microscopic and macroscopic instabilities in finitely strained fiber-reinforced elastomers. J Mech Phys Solids 58(11):1776–1803
16. Miehe C (2002) Strain-driven homogenization of inelastic microstructures and composites based on an incremental variational formulation. Int J Numer Methods Eng 55(11):1285–1322
17. Miehe C, Lambrecht M (2003) A two-scale finite element relaxation analysis of shear bands in non-convex inelastic solids: small-strain theory for standard dissipative materials. Comput Methods Appl Mech Eng 192(5):473–508
18. Moraleda J, Segurado J, LLorca J (2009) Finite deformation of incompressible fiber-reinforced elastomers: a computational micromechanics approach. J Mech Phys Solids 57(9):1596–1613
19. Segurado J, Llorca J (2002) A numerical approximation to the elastic properties of sphere-reinforced composites. J Mech Phys Solids 50(10):2107–2121
20. Simo JC, Taylor RL, Pister KS (1985) Variational and projection methods for the volume constraint in finite deformation elasto-plasticity. Comput Methods Appl Mech Eng 51(1):177–208
21. Sukumar N, Tabarraei A (2004) Conforming polygonal finite elements. Int J Numer Methods Eng 61(12):2045–2066
22. Sussman T, Bathe KJ (1987) A finite element formulation for nonlinear incompressible elastic and inelastic analysis. Comput Struct 26(1):357–409
23. Webb J (1990) Imposing linear constraints in finite-element analysis. Commun Appl Numer Methods 6(6):471–475
24. Wriggers P (2008) Nonlinear finite element methods, vol 4. Springer, Berlin
25. Zienkiewicz OC, Taylor RL (2005) The finite element method for solid and structural mechanics. Butterworth-Heinemann, Oxford